Available online at www.CivileJournal.org

Civil Engineering Journal

(E-ISSN: 2476-3055; ISSN: 2676-6957)

Vol. 11, No. 08, August, 2025

Web-Crippling Behaviour of Cold-Formed Screw Fastened Rectangular Hollow Flange Z-Section Beams Under Two-Flange Load Cases

Koppala Siva [1], Joseph Antony Visuvasam [1*]

[1] School of Civil Engineering, Vellore Institute of Technology, Tamil Nadu 632014, India.

Received 23 January 2025; Revised 17 July 2025; Accepted 23 July 2025; Published 01 August 2025

Abstract

This study investigates to update the web-crippling coefficients of cold-formed screw-fastened hollow flange Z-section (SFHZ) beams under End-Two-Flange (ETF) and Interior-Two-Flange (ITF) loading conditions. As coefficients are available in AISI standards to estimate the web crippling capacity of Z-sections, experimental program is carried out on 48 number of SFHZ specimens. An extensive parametric study considering the effects of web slenderness, material strength, and support length is conducted for 240 finite element models. Both experimental results and Finite Element Analysis (FEA) were used to predict web-crippling capacities and verified with current AISI predictions. The findings reveal that existing specifications are un-conservative for both ETF and ITF load cases. The parameters such as web height-to-thickness, inside bend radius-to-thickness, and bearing length-to-thickness ratios are the key factors influencing the prediction of web crippling capacity of SFHZ sections. As a result, the study proposes updated web-crippling coefficients that offer improved accuracy in predicting SFHZ section performance under two-flange loading conditions.

Keywords: Cold-Formed Steel; Screw-Fastened Rectangular Hollow Z-Section; Web-Crippling, Experimental Investigation; Numerical Analysis, Two-Flange-Loading.

1. Introduction

Cold-formed steel (CFS) structural members are increasingly being utilized in construction due to their cost-effectiveness, versatility, and greater strength-to-weight ratio [1]. The members bring several advantages, such as the simplicity of fabrication, light structure, and efficient transportation, that enable them to be the preferred substitute for hot-rolled sections [2]. The commonly used structural systems of CFS in low-rise residential and office buildings include C-sections, Z-sections, hat sections and I-sections [3].

Experimental investigations on web-crippling of CFS beams began by Wintr & Pian's [4]. Standardized design equations now stem from AISI S100-16 [5], AS/NZS 4600 [6], and Canada S136-94 [7] specifications, however coefficients underwent successive refinements following landmark studies by Hetrakul & Yu [8], Santaputra [9], and Bhakta et.al [10]. Since then, dozens of experimental campaigns targeted unlipped channel sections effects [11-16], including early work in the 1970s and more recent high-strength tests, while lipped channel investigations explored flange stiffening and lip geometry [17-21]. Z-sections; both unlipped [22-24] and lipped [25-32] have received focused attention, alongside complementary studies on hat [33, 34] and I-section [35, 36] profiles. Analytical approaches range from simple plastic mechanism formulations [37, 38] to cutting-edge swarm-optimization algorithms and in-depth- parametric sweeps (yield mechanism) of thickness, bend radius, and bearing length [39, 40]. This body of research has enriched coefficient tables, sharpened failure predictions, and laid the groundwork for more economical and safety-conscious CFS designs.

* Corresponding author: visuvasam.j@vit.ac.in

http://dx.doi.org/10.28991/CEJ-2025-011-08-07

Web-crippling behaviour in cold-formed steel (CFS) sections has long received attention owing to its critical influence on structural safety and material efficiency. Hussein & Hussein [41] conducted a comprehensive investigation on the effects of lip length and inside radius-to-thickness ratio on buckling resistance of CFS profiles. Finite element analyses of 176 specimens demonstrated that increasing the lip length significantly elevated the elastic buckling load and moment capacity, prompting a minimum lip length of 15 mm in beams and columns to avert premature local buckling. In a follow-up review [42], Hussein and Hussein surveyed additional geometric and material variables that influence CFS member strength in construction scenarios. The study identified the discrepancies between the AISI S100 and AS/NZS 4600 provisions, particularly in conservative predictions for composite and built-up- assemblies. Young & Ellobody [23] compared these profiles under End-Two-Flange and Interior-Two-Flange loading, revealing that both the bearing length and load arrangement critically influence the web-crippling capacity. Dwivedi & Vyavahare [43] introduced revised web-crippling coefficients, demonstrating that North American specifications tend to overestimate capacity, whereas European codes align more closely with the observed behavior. Meanwhile, Taimur et al. [44] examined hot-rolled- rectangular hollow sections featuring web perforations and tested 20 specimens under both ITF and ETF conditions. Finite element models and parametric studies were used to quantify the effects of hole diameter and offset on crippling resistance. From this analysis, targeted design recommendations emerged, supported by reliability assessments, to ensure a robust performance. Collectively, the studies provide a path toward more economical, data-driven design approaches for cold-formed- steel members.

AISI S100 provides the empirical equation for evaluate the web crippling strength is given by Equation 1.

$$P_n = C t_w^2 f_{yw} \sin\theta \left(1 - C_w \sqrt{\frac{d_1}{t_w}}\right)\left(1 - C_r \sqrt{\frac{r_i}{t_w}}\right)\left(1 + C_{lb} \sqrt{\frac{l_b}{t_w}}\right) \quad (1)$$

This empirical equation considers relevant parameters such as the inner bent radius (R), loading plate length (l_b), web height (h), thickness (t), and angle between the web plane and bearing surface. It also accounts for the yield strength (f_y) and web crippling coefficients, including the ratio of the inner bent radius to the web thickness (C_R), web slenderness coefficient (C_h), bearing length-to-thickness coefficient (C_{lb}), and overall coefficient (C).

The rising demand for economical structural solutions has driven innovation in CFS profiles, inspiring designs such as sigma sections, space frames, and hollow flange-members [45, 46]. Screw-fastened rectangular hollow flange-Z-section (SFHZ) has emerged as a cost-effective successor [13, 47]. By substituting extensive welding with self-drilling screws, SFHZ beams streamline assembly, reduce heat input, and reduce labour expenses while maintaining high strength ratios [48, 49]. This strategy also addresses fabrication complexity by positioning SFHZ sections as a sustainable, high-performance choice for modern construction. Figure 1 shows the fully assembled SFHZ specimen. The investigation focused on the web-crippling resistance of these screw-fastened Z-sections under End-Two-Flange (ETF) and Interior-Two-Flange (ITF) loading. Web crippling represents a critical failure mechanism in thin-walled steel profiles, where point loads trigger localized deformations that significantly reduce the load capacity. Prior studies revealed that established design provisions, particularly AISI S100 and AS/NZS 4600, tend to underestimate the strength of cold-formed- members [50, 51]. By adopting self-drilling- screws instead of traditional welding or riveting, connections can achieve higher uniformity and tighter fit, simplify assembly, and facilitate maintenance. A comprehensive evaluation through both experimental testing and numerical modelling underpins these findings, ensuring that the refined design recommendations align with real-world- performance. This approach advances cold-formed- steel design practices, offering a pathway for more efficient, cost-effective-, and reliable structural solutions to modern construction demands.

Figure 1. Cold-formed screw-fastened hollow Z-section beam (SFHZ)

Rivet-fastened Rectangular Hollow Flange Channel Beams (RHFCBs) incorporate supplementary lip stiffeners that markedly improve the buckling resistance, structural rigidity, and load-bearing- capacity while streamlining handling

and on-site fabrication. Steau et al. [52] investigated web-crippling phenomena and ultimate strength for RHFCBs under both End-Two-Flange (ETF) and Interior-Two-Flange (ITF) loading. Their study revealed that failure modes arise from a combination of flange crushing and localized web crippling. When benchmarked against AISI S100 and AS/NZS 4600 design curves, the existing equations proved overly conservative for riveted RHFCBs in the ETF and ITF scenarios. To address this gap, Steau et al. [52] derived refined empirical expressions tailored to the unique geometry and connection details of these built-up- members, yielding far more accurate strength predictions. Keerthan & Mahendran [53] examined the web-crippling behavior of Lite Steel beams under End-One-Flange (EOF) and Interior-One-Flange (IOF) conditions. Twenty-three full scale tests demonstrated that the current AS/NZS 4600 and AISI S100 provisions substantially underestimate the actual capacity. Drawing on experimental insights, they proposed enhanced design equations within the Direct Strength Method framework, offering an improved alignment with the observed performance. These combined advances lay the groundwork for developing more economical and reliable cold-formed steel design guidelines.

Recent efforts to streamline the production of rectangular hollow flange channel sections have refined cold-forming techniques and integrated dual-electric resistance-welding, boosting the throughput and material consistency. Wanniarachchia & Mahendran [54] evaluated these colored rectangular hollow flange beams (RHFBs) against AS/NZS 4600 and AISI S100 criteria, showing that applying a screw spacing reduction factor ensures reliable strength predictions. Testing indicated that increasing the screw spacing from 50 to 100 mm caused only a minor 5 % decrease in moment capacity, underscoring the robustness of the section. The Direct Strength Method (DSM) also delivered conservative yet accurate moment estimates for both screw-fastened and welded configurations. Future research will examine alternative RHFB geometries to optimize load-to-weight ratios and enhance the overall efficiency. In parallel, Ishqy et al.[55] investigated the shear behaviour in RHFCBs with non-circular web openings. Combined experimental and finite element studies revealed that such openings could reduce the shear capacity by up to 70 %, highlighting the delicate balance between weight savings and structural performance. These insights pave the way for more nuanced design strategies that improve efficiency and safety in contemporary cold-formed- steel applications.

Screw connections promote a uniform load transfer, strengthen the joint integrity, and simplify maintenance across a wide range of structural applications. Maali et al. [56] increase in beam thickness increases the strength (F_{max}) and energy-absorbing ability of cold-formed steel (CFS) screw connections but slightly reduces their rotation capacity (θF_{max}). Finite element analysis (FEA) was extremely in agreement with experimental results, highlighting the importance of tailoring connection design to specific loading scenarios to ensure optimal performance. In a complementary investigation, Li et al. [57] influence parameters such as screw diameter, sheet thickness, edge angle, end distance, and screw configuration. The connection having a thickness ratio of 1.0 would most probably be the pulling-out failure because the thinner sheet was unable to yield enough pull-out resistance. Punching failure was more prevalent at a 1.5d end distance, causing shear strength to decrease by about 20%.

The integration of full-scale- tests and nonlinear finite element simulations has enabled a comprehensive evaluation of web-crippling in cold-formed screw-fastened hollow-flange beam (SFHZ) section design (see Figure 2).

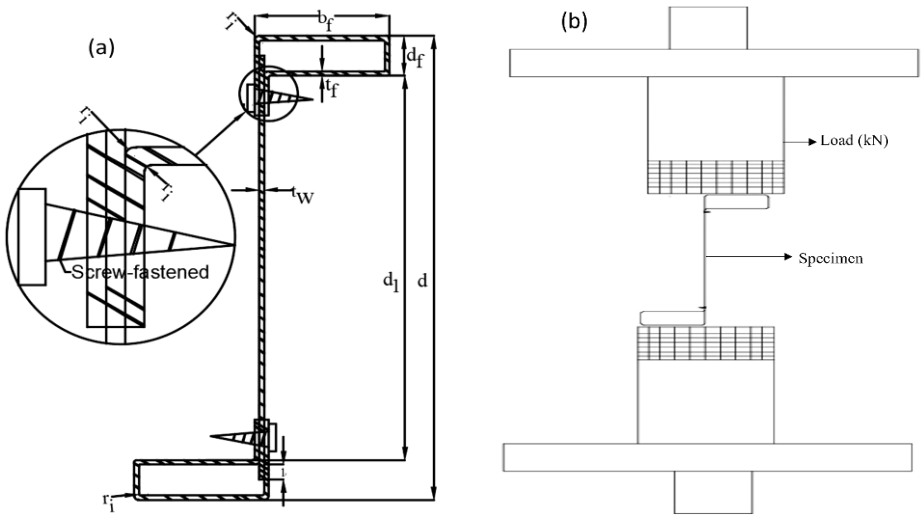

Figure 2. (a) Dimensional of SFHZ-section, (b) Test setup of SFHZ-section

End-Two-Flange and Interior-Two-Flange loading conditions are considered for the experimental study on 48 specimens to probe the effects of web slenderness, inner bent radius, and bearing length on crippling resistance (yield mechanism). The validated numerical models reproduced buckling and failure patterns with high fidelity. Adjustments to traditional design formulas, informed by these findings, yield more precise capacity estimates for the SFHZ beams.

A thorough review of the existing literature underscores the urgent need for refined web-crippling prediction tools in cold-formed- steel design. The calibration of new coefficients against both experimental data and finite element analyses bridges critical gaps in the current code provisions. This dual method not only enhances the reliability of capacity predictions but also paves the way for optimized, resource-efficient- structural solutions. The resulting design guidelines promise safer and more economical CFS applications using diverse engineering approaches.

2. Research Methodology

This study examines the web-crippling behaviour of cold-formed SFHZ sections based on extensive parametric studies using experimental testing and finite element analysis (FEA). To compare their structural performances, 48 specimens were chosen and tested under end-two-flange (ETF) and interior two-flange (ITF) loading conditions. Figure 3 shows a workflow chart representing the methodological steps and processes. This study compared new web crippling coefficients with experimental data and existing design equations, focusing on cold-formed steel-lipped channel beams subjected to one-flange loading conditions. FEA was carried out considering the validation of experimental results identifying the failure modes, stress distributions, and load-displacement responses. Parametric analysis was carried out to understand the influence of important geometric parameters, such as thickness, bend radius, and bearing length, on the web-crippling strength. The output obtained was compared with the AISI S100 and AS/NZS 4600 standard predictions to analyse their conservatism and accuracy. A reliability analysis is conducted to ensure the accuracy in predicting the web crippling capacity of the SFHZ sections. The study concludes with enhanced design recommendations that guarantee more precise web-crippling strength predictions for cold-formed SFHZ sections for engineering applications.

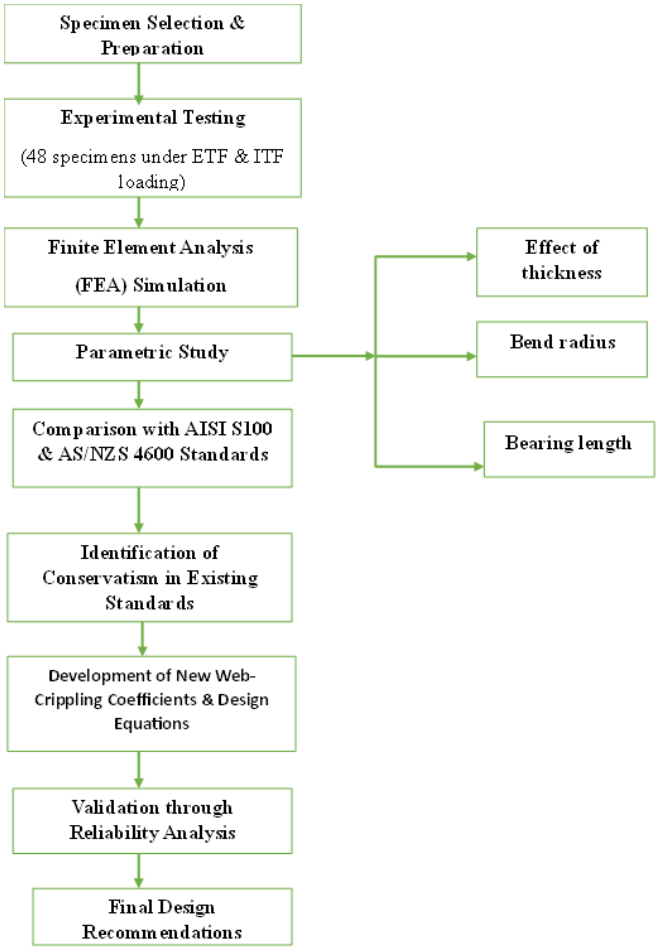

Figure 3. Workflow of methodology

2.1. Experimental Investigation

An extensive experimental investigation was performed to analyse the structural response of 48 numbers of SFHZ beams under ETF and ITF loading conditions. This study examined the structural response under several loading and boundary conditions, emphasizing the determination of the stress concentration zones and sites of possible failure. The results add to the knowledge of the structural integrity and effect of design alterations on the performance and reliability of SFHZ beams.

Studies have shown that current web crippling design equations for cold-formed steel sections may be conservative, highlighting the need for computational modelling to capture geometric and material imperfections. Janarthanan et al. [11] conducted experimental and finite element analysis on lipped channel sections and found that AISI-S100 underestimated web crippling strength by up to 18% for sections with high web slenderness. Refining web crippling coefficients can enhance the accuracy, especially for sections with high slenderness ratios. Further research is needed to incorporate cold-working effects and develop standardized procedures for improved design reliability

The experimental analysis was based on the North American specifications, and the ETF and ITF web-crippling load conditions were tested. Two Z-sections (Figure 4) were joined with rigid components to achieve torsional and lateral stability. The Z-sections had a constant depth (d) of 150 mm; flange breadth (b_f) of 55 mm; lip depth (d_f) of 18 mm; and thicknesses (t) of 1.2 mm, 1.6 mm, and 2.0 mm. These experiments were conducted to further enhance the understanding of web-crippling behaviour and design recommendations for safer structural design.

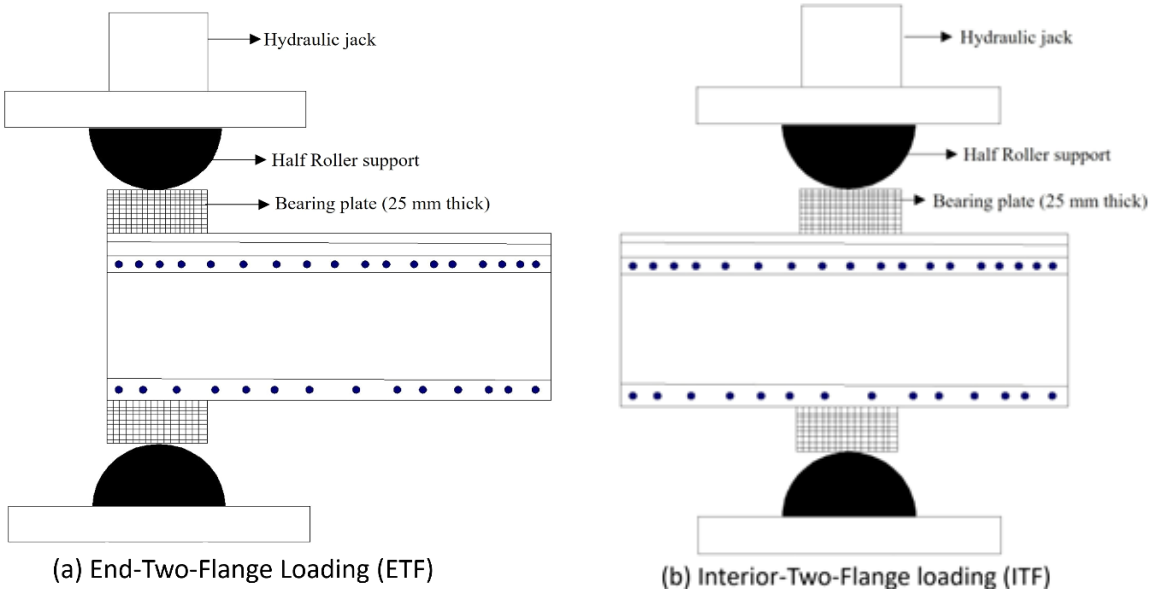

Figure 4. Load cases for Web-crippling test

2.2. Test Setup

2.2.1. Experimental Configuration of ETF Loading

For the ETF loading test, a Z_1 specimen (200×55×18×1.2 mm with dimensions $r_i3 \times l_b100$ mm) was utilized (Figure 5). The elongations of the steel specimens under the ETF loading conditions were measured using a rotary encoder. The testing machine delivered a maximum load of 1000 kN and recorded elongations of up to 250 mm. The specimen, 1.2 mm thick and 55 mm wide, measured a maximum load of 5.73 kN. The rotary encoder ensured accurate elongation measurements, thereby increasing the reliability and validity of the experimental results.

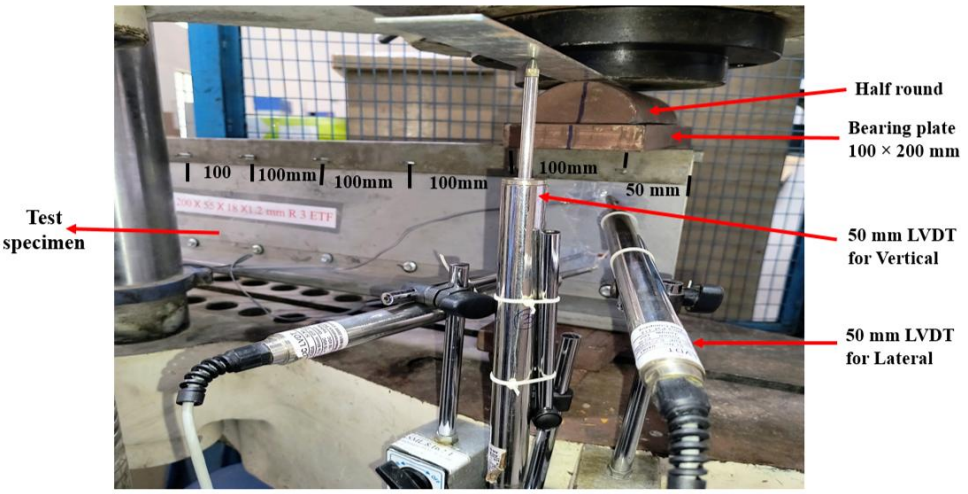

Figure 5. ETF Loading (Z_1 200×55×18×1.2×$r_i3 \times l_b100$ mm)

2.2.2. Experimental Configuration for ITF Loading

For the ITF loading test, a Z_2 specimen (150 mm ×55 mm ×18×1.6 mm with dimensions $r_i3\times l_b100$ mm) was tested (Figure 6). In a similar ETF setup, elongation was measured using a rotary encoder. The specimen 1.6 mm thick and 55 mm wide had a maximum applied load of 1000 kN with an elongation capability of up to 250 mm. The maximum load in the experiment was 14.96 kN. The rotary encoder ensured accurate elongation measurements, which made it possible to precisely analyse the behaviour of the material under ITF loading conditions. shows the load-elongation relationship for ITF loading.

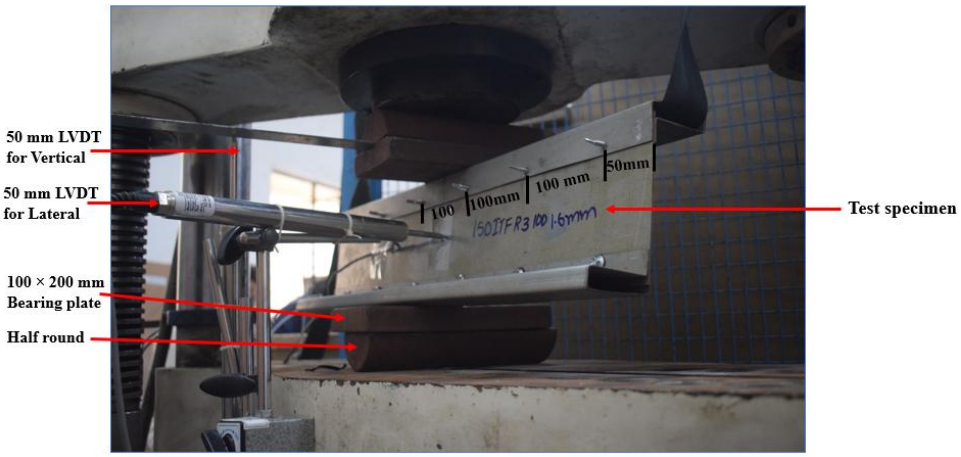

Figure 6. ITF Loading (Z_2 150×55×18×1.6×$r_i3\times l_b100$ mm)

2.3. Tensile Coupon Test

As per the IS 513-2016 standards, a zinc coating was applied to all the cold-formed steel specimens. Tensile coupon testing for each thickness was performed according to ISO 6892-1-2018 to determine the elastic limit and critical fracture stress of Z-sections [58]. The rectangular plates were sheared parallel to the Z-section axis to obtain standard tensile coupons. The thickness and width were measured at three points along the gauge length, and the average values were used to compute the mechanical properties.

Figure 7 depicts the tensile coupon specimen details, which reveal the material properties employed for estimating the structural response of the SFHZ beams under ETF and ITF loading conditions. The mechanical properties of cold-formed steel, including modulus thicknesses (1.2 mm and 1.6 mm), were revealed through tensile coupon test results. The thinner gauges (1.2 mm) exhibited a higher yield strength (457 MPa) and critical fracture stress (770 MPa) but lower ductility (32.5% elongation); hence, they were strong but not very deformable. In contrast, thicker specimens (2.0 mm) provided lower strength (226 MPa yield, 315 MPa ultimate) with higher ductility (56.5% elongation), which supported greater deformation before failure. The modulus of elasticity (E) decreases with increasing thickness, indicating a small reduction in stiffness [28]. These findings will enable the design of ideal Z-section shapes with application-specific strength and ductility requirements for structural loading.

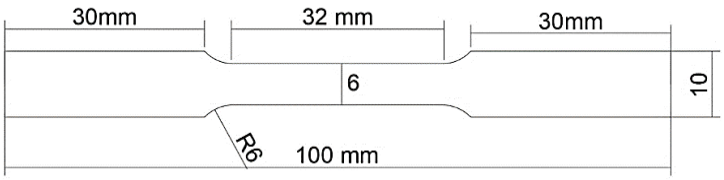

Figure 7. Specimen details of tensile coupon test

Table 1 presents the tensile coupon test results, such as Modulus of elasticity (E), elastic limit (f_{yw}), Critical fracture stress (f_u), and gauge length (ε_u). The mechanical properties of CFSFHZ sections with different thicknesses (1.2 mm, 1.6 mm, and 2.0 mm) were revealed through tensile coupon test results. The thinner gauges (1.2 mm) exhibited higher yield strength (457 MPa) and ultimate strength (770 MPa), and lower ductility (32.5% elongation). Moreover, thicker specimens (2.0 mm) provided lower strength (226 MPa yield, 315 MPa ultimate) with higher ductility (56.5% elongation), which supported greater deformation before failure. The modulus of elasticity (E) decreases with increasing thickness, indicating a small reduction in stiffness [59]. These findings will enable the design of ideal Z-section shapes with application-specific strength and ductility requirements for structural loading.

Table 1. Tensile coupon test results

t (mm)	E (GPa)	f_{yw} (MPa)	f_u (MPa)	ε_u (%)
1.20	248	457	770	32.5
1.60	217	248	354	52.0
2.0	184	226	315	56.5

2.4. Web Crippling test for Two-Flange Load Cases

The web-crippling performance of the CFSFHZ sections was evaluated through experimental testing under two-flange loading conditions. The test setup comprised a loading frame in which a hydraulic jack was positioned centrally to apply the web-crippling load. A Universal Testing Machine (UTM) applied a force through a loading plate, which was displaced by 20 mm. A load sensor was connected to a data acquisition (DAQ) system to measure the load with a high degree of accuracy.

Strain gauges were attached to either side of the CFSFHZ-section web to measure ETF and ITF strains. Inductive Transducers were attached below the loading plate to measure the vertical displacement. The transducers were arranged such that the lateral and vertical displacements could be measured accurately, and the deformation patterns and structural responses could be adequately assessed. SFHZ sections, 18 mm high and 55 mm wide, were screw-fastened on web plate of 100 mm. The heights of all the specimens were 150- and 200-mm. Zinc-coated CFS was used to fabricate specimens with 1.2 mm, 1.6 mm, and 2.0 mm thicknesses. Tensile coupon tests were conducted prior to the web-crippling tests to determine the critical fracture stress of the steel sheets utilized for the experiments.

Tables 2 and 3 provide SFHZ specimens under ETF and ITF loading conditions. The specifications include overall depth (d), clear web heights (d_1), Flange breadth (b_f), flange depth (d_f), flange gauge (t_f), web thickness (t_w), and elastic limit (f_{yw}). The web-crippling test results were utilized to assess the structural response of the SFHZ beams and validate numerical models developed for future analysis.

Table 2. Web crippling test specimen under loading case of ETF

S. No.	Screw-Fastened Hollow Z-section Beam ($d\times b_f\times d_f\times t_f\times t_w$)	d_1 (mm)	d_1/t_w	f_{yw} (MPa)	r_i (mm)	l_b (mm)	L (mm)	P_{EXP} (kN)
1	150×55×18×1.2×1.2	114	95.00	457	3	50	342	4.85
2	200×55×18×1.2×1.2	164	136.67	457	3	50	492	4.52
3	150×55×18×1.6×1.6	114	71.25	248	3	50	342	6.12
4	200×55×18×1.6×1.6	164	102.50	248	3	50	492	5.69
5	150×55×18×2.0×2.0	114	57.00	226	3	50	342	8.82
6	200×55×18×2.0×2.0	164	82.00	226	3	50	492	8.27
7	150×55×18×1.2×1.2	114	95.00	457	3	100	342	6.60
8	200×55×18×1.2×1.2	164	136.67	457	3	100	492	5.73
9	150×55×18×1.6×1.6	114	71.25	248	3	100	342	7.95
10	200×55×18×1.6×1.6	164	102.50	248	3	100	492	7.32
11	150×55×18×2.0×2.0	114	57.00	226	3	100	342	9.64
12	200×55×18×2.0×2.0	164	82.00	226	3	100	492	8.96
13	150×55×18×1.2×1.2	114	95.00	457	4	50	342	4.57
14	200×55×18×1.2×1.2	164	136.67	457	4	50	492	4.18
15	150×55×18×1.6×1.6	114	71.25	248	4	50	342	5.84
16	200×55×18×1.6×1.6	164	102.50	248	4	50	492	5.34
17	150×55×18×2.0×2.0	114	57.00	226	4	50	342	8.16
18	200×55×18×2.0×2.0	164	82.00	226	4	50	492	7.98
19	150×55×18×1.2×1.2	114	95.00	457	4	100	342	5.19
20	200×55×18×1.2×1.2	164	136.67	457	4	100	492	4.82
21	150×55×18×1.6×1.6	114	71.25	248	4	100	342	6.97
22	200×55×18×1.6×1.6	164	102.50	248	4	100	492	5.97
23	150×55×18×2.0×2.0	114	57.00	226	4	100	342	9.15
24	200×55×18×2.0×2.0	164	82.00	226	4	100	492	8.50

Table 3. Web crippling test specimen details under loading case of ITF

S. No.	Screw-Fastened Hollow Z-section Beam ($d \times b_f \times d_f \times t_f \times t_w$)	d_1 (mm)	d_1/t_w	f_{yw} (MPa)	r_i (mm)	l_b (mm)	L (mm)	P_{EXP} (kN)
1	150×55×18×1.2×1.2	114	95.00	457	3	50	570	9.62
2	200×55×18×1.2×1.2	164	136.67	457	3	50	820	9.02
3	150×55×18×1.6×1.6	114	71.25	248	3	50	570	11.98
4	200×55×18×1.6×1.6	164	102.50	248	3	50	820	11.02
5	150×55×18×2.0×2.0	114	57.00	226	3	50	570	16.80
6	200×55×18×2.0×2.0	164	82.00	226	3	50	820	16.48
7	150×55×18×1.2×1.2	114	95.00	457	3	100	570	10.81
8	200×55×18×1.2×1.2	164	136.67	457	3	100	820	10.17
9	150×55×18×1.6×1.6	114	71.25	248	3	100	570	14.96
10	200×55×18×1.6×1.6	164	102.50	248	3	100	820	13.54
11	150×55×18×2.0×2.0	114	57.00	226	3	100	570	20.17
12	200×55×18×2.0×2.0	164	82.00	226	3	100	820	19.26
13	150×55×18×1.2×1.2	114	95.00	457	4	50	570	7.85
14	200×55×18×1.2×1.2	164	136.67	457	4	50	820	7.63
15	150×55×18×1.6×1.6	114	71.25	248	4	50	570	10.83
16	200×55×18×1.6×1.6	164	102.50	248	4	50	820	10.09
17	150×55×18×2.0×2.0	114	57.00	226	4	50	570	15.19
18	200×55×18×2.0×2.0	164	82.00	226	4	50	820	14.86
19	150×55×18×1.2×1.2	114	95.00	457	4	100	570	9.98
20	200×55×18×1.2×1.2	164	136.67	457	4	100	820	9.48
21	150×55×18×1.6×1.6	114	71.25	248	4	100	570	12.57
22	200×55×18×1.6×1.6	164	102.50	248	4	100	820	11.86
23	150×55×18×2.0×2.0	114	57.00	226	4	100	570	18.92
24	200×55×18×2.0×2.0	164	82.00	226	4	100	820	18.19

Figure 8 presents a failure analysis of the experimental testing conducted on ETF Z_1 (200×55×18×1.2 mm) and ITF Z_2 (150×55×18×1.6 mm). Figure 9 displays the load-vertical and lateral deflection curves of experimental (EXP) for the Z_1 (ETF) and Z_2 (ITF) sections. The curves show the structural response of the sections to gradually applied loads to failure and the differences in their elastic and plastic deformation characteristics. In Figure 9-a (ETF–Z_1), the load-deflection curve first shows a linear region of elastic behaviour, and the structural response remains proportional to the applied load. When the deflection exceeded 4 mm, the load experienced a further increase, and the response entered the plastic deformation region, in which permanent deformations occurred. The ultimate failure is observed after approximately 20 mm of deflection, which means that the Z_1 section under ETF loading exhibits high strength before it reaches its crippling limit.

Figure 8. Failure Pattern Analysis in ETF (Z_1) and ITF (Z_2) Experimental Studies

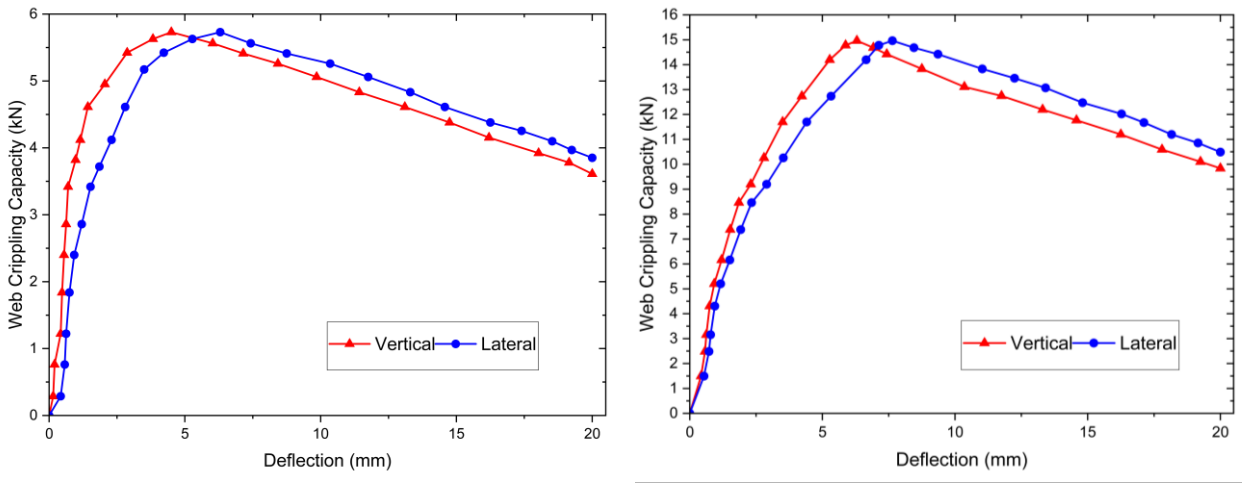

(a) Load-deflection plot for Z_1 ETF

(b) Load-deflection plot for Z_2 ITF

Figure 9. Comparison of failures of experimental testing ETF and ITF load cases

Similarly, Figure 9-b (ITF–Z_2) exhibits a similar trend, but with a higher initial stiffness and a more gradual slope to plastic deformation. The linear elastic phase increases to 6 mm of deflection, after which yielding occurs. Ultimate failure occurs beyond 20 mm of deflection, as in ETF loading; however, the ITF section shows a slightly greater structural resistance before total failure. The small discrepancies observed may be attributed to fabrication tolerances, small geometric defects, or variations in material properties. The results revealed that ITF sections can withstand slightly higher deformations prior to failure as a result of better load distribution, thus being more resistant to web crippling than ETF sections.

2.5. Experimental Results

The structural performance of the cold-formed screw-fastened rectangular hollow-flange Z-sections was comprehensively assessed using a set of experimental tests. This study focused on two specimen configurations: Z_1 (200×55×18×1.2 mm) and Z_2 (150×55×18×1.6 mm). The specimens were tested under controlled loading conditions for both end-two-flange (ETF) and interior-two-flange (ITF) load cases, which mimicked actual structural stress cases.

The main goals of the experiments were to examine the stability, deformation behaviour, and stress distribution of the samples under various loading conditions. By closely monitoring the response of the specimens to loads, this study aimed to elucidate the crucial failure mechanisms, variations in the load-carrying capacity, and web-crippling modes. These results provide important knowledge for optimizing cold-formed Z-sections, emphasizing their use in light steel structures. The experimental approach used in this study was compression testing to quantify the vertical and lateral deflections of the Z-sections with rising loads. The load-deflection response was monitored to evaluate how each section deformed over time until failure. Figure 9 presents the results of these tests, where the load-deflection curves indicate the structural performance differences under ETF and ITF loading. Plastic deformation followed the initial elastic deformation stage in each instance, resulting in web-crippling failure. These observations are significant for improving the design specifications and engineering guidelines of cold-formed steel Z-sections. From the mechanical response and failure mechanisms, structural engineers can improve the predictions of load-carrying capacity, which contributes to safer and more efficient steel structures in the construction and industrial sectors.

2.6. Numerical Investigation (FEM Model)

A full-scale finite element model of the cold-formed SFHZ was constructed in ABAQUS [60, 61] to capture its behaviour under ETF and ITF loading. A static general procedure was adopted for the nonlinear analysis to avoid the high computational cost of explicit solvers. This approach effectively simulates the buckling initiation, stress fields, and deformation modes observed in physical tests, ensuring close agreement with the experimental findings while maintaining manageable resource demands. The fidelity of the model was enhanced by the nonlinear material behaviour, and the boundary conditions mirrored the experimental setup.

2.6.1. Finite Element Model Setup

2.6.1.1. Element Type and Mesh Size

Finite element analysis of thin-plate buckling relies on specialized shell elements such as S4, S4R, S4RS, and S4RSW. S4R elements, featuring quadrilateral, doubly curved thin-shell- geometries, are particularly adept at modelling screw-fastened, cold-formed sections [62]. Each S4R node offers six degrees of freedom complemented by an internal hourglass-control algorithm to prevent spurious distortions. The four-node- bilinear quadrilateral R3D4 element defines a discrete rigid body with six reference point- degrees of freedom for rigid components such as bearing plates and angle sections. Integrating these elements within a coherent mesh framework enhances the capture of bending–torsion interactions. The mesh density directly influences the resulting fidelity: uniform 5 mm × 5 mm elements map general stress fields, while targeted 1 mm × 5 mm refinements along corners and web zones identify peak stresses and incipient buckling. Selective integration strategies further balance the computational load by simplifying low-strain- regions. This mesh tailoring delivers detailed insights into local deformation patterns while preserving the overall model efficiency, ensuring accurate local and global buckling behaviour predictions through comparison with experimental results.

2.6.2. Characteristics of Materials and Stress-Strain Behaviour

Accurate finite element analysis depends on precise material characterization. The mechanical properties derived from tensile testing of cold-formed- steel sheets formed the basis for the simulation inputs [63]. Key parameters included the modulus of elasticity (E) to define stiffness, elastic limit (f_{yw}) marking the onset of plastic deformation, and critical fracture stress (f_u) representing the ultimate strength before failure. Additionally, the strain-hardening- curve captured the post-yield- material strengthening. Incorporating the experimentally determined values into the numerical model ensured that the stress–strain responses, deformation patterns, and failure predictions closely mirrored the observed behaviour under loading conditions.

The engineering stress-strain curve ($\sigma - \varepsilon$) from the tensile tests was transformed into true stress (σ_{true}) and logarithmic plastic strain (ε_{true}) for proper FEA input. The transformation was performed using Equations 2 and 3:

$$\sigma_{true} = \sigma(1 + \varepsilon) \quad (2)$$

$$\varepsilon_{true} = ln(1 + \varepsilon) - \frac{\sigma_{true}}{E} \quad (3)$$

2.6.3. Boundary Conditions, Contact and Load Application

A meticulous definition of boundary conditions and load applications is crucial for reproducing real-world behaviour within finite element models. Figure 10 shows the imposed loading and boundary conditions used in the FEA model. This framework fully constrains the support plates against translations along the X-, Y-, and Z-axes, preventing unintended movement under high loads. The rotational degrees of freedom about the Y- and Z-axes were similarly locked, preserving the structural stability during the simulation of compressive forces. The loading plate underwent comparable restrictions: translational motion along the X- and Z-directions and rotations around the Y- and Z-axes were fixed to emulate the rigidity of the experimental fixtures. A controlled vertical displacement of 20 mm was applied at the designated reference point on the loading plate to accurately reproduce the compression stroke observed in the physical tests. Contact interactions adopted a master-slave approach, assigning the bearing plates as master surfaces and the Z-section as slave surfaces to ensure robust convergence [64]. A uniform friction coefficient 0.4 was imposed at all contact interfaces, capturing the sliding resistance measured during laboratory trials. A comparison of the load-deflection curves and failure patterns confirmed that the numerical predictions matched the experimental results within a minimal margin of error. Such an alignment reduces reliance on repeated physical tests, enhances design efficiency, and reinforces confidence in the model's validity for broader parametric investigations.

2.6.4. Initial Geometric Imperfections Influence

The manufacturing of cold-formed steel often introduces subtle geometric asymmetries that influence buckling and web-crippling behaviour [65]. To evaluate these imperfections, the finite element model incorporated an initial out-of-plane flaw equal to one-150th of the section depth (h/150). A subsequent analysis revealed that such minor deviations exerted a negligible effect on the ultimate web-crippling strength. Consequently, practical engineering simulations may omit the explicit representation of these small-scale- geometric irregularities without sacrificing accuracy. This finding streamlines the modelling process, reducing the complexity and computational effort while preserving reliable predictions of thin-walled- steel performance under concentrated loads [41]. By emphasizing the robustness of the FEA approach, minor manufacturing defects are largely inconsequential for design-level- assessments.

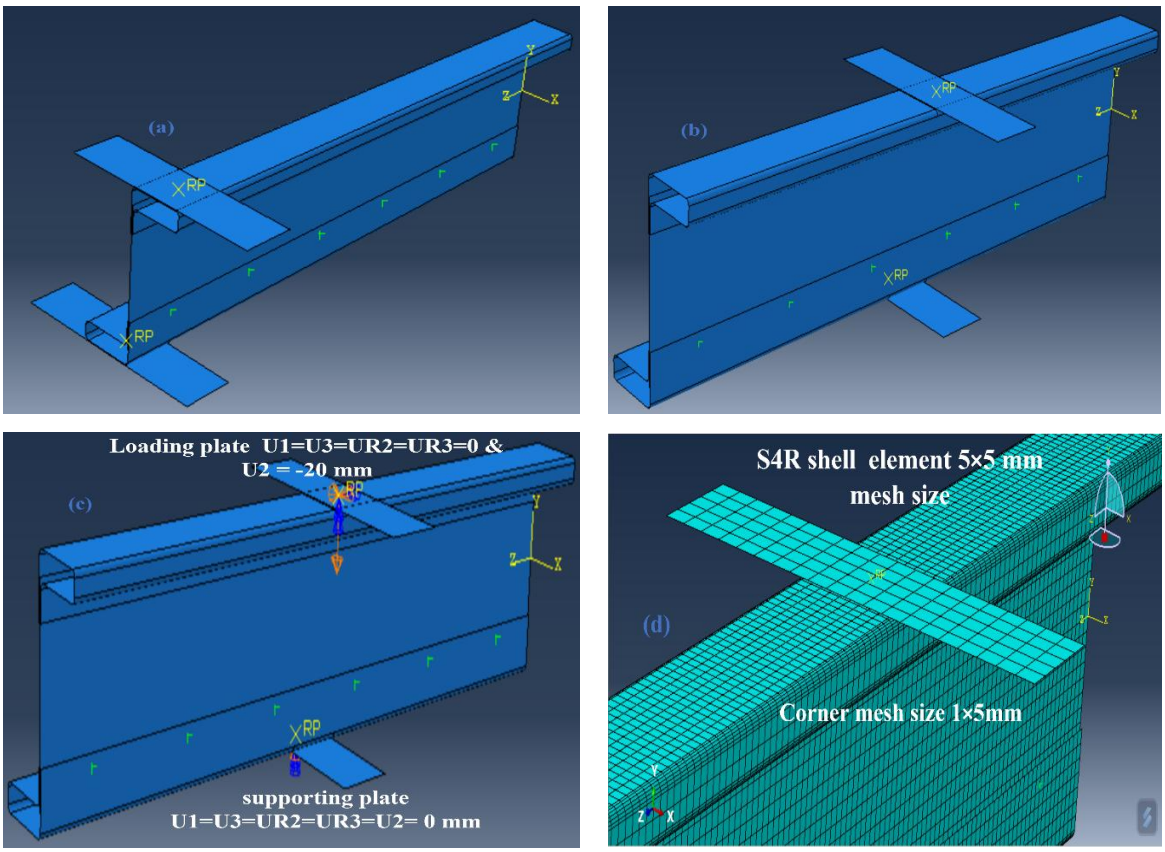

Figure 10. Loading & boundary conditions (a) ETF loading (b) ITF loading (c) Boundary conditions (d) Meshed steel section and bearing plate

2.6.5. Effect of Lip Stiffeners on Web Crippling Resistance

Cold-formed Z-sections rely on lip stiffeners to delay local buckling and bolster structural rigidity under concentrated loads. The angle of these stiffeners (θ_l) relative to the flange is critical: a perpendicular orientation (90°) delivers substantial reinforcement by effectively redistributing stress, whereas shallower inclinations (45°) provide minimal support, allowing web crippling to be initiated at lower load levels. Incremental testing across angles from 45° to 90° confirmed that only right-tangled- stiffeners yield meaningful gains in buckling resistance, while sloped lips offer negligible improvement. High-fidelity- finite element simulations in ABAQUS replicated the experimental failure modes and stress distributions with impressive accuracy. Quadrilateral S4R shell elements, chosen for their six degrees of freedom and built-in- hourglass control, captured coupled bending–torsion behaviour in thin-walled- profiles. The R3D4 discrete rigid elements define the bearing plates and connector interfaces. Mesh density proved pivotal: a uniform 5 mm×5 mm grid mapped global stress fields, while a refined 1 mm × 5 mm mesh in the corner and web regions pinpointed stress concentrations and buckling initiation sites.

This adaptive meshing strategy balances the computational load with the detailed local accuracy. Incorporating real-world- material data strengthened the predictive reliability. The tensile test results provided the modulus of elasticity, elastic limit, critical fracture stress, and strain hardening- curves, which were directly embedded into the constitutive definitions of the model. Boundary constraints mirrored the laboratory setup—support plates were fully fixed in translations and rotations, and the loading plate was restricted in all but a 20 mm vertical displacement. Master-slave contact formulation with a friction coefficient of 0.4, faithfully reproduced the interface interactions. Introducing a small geometric imperfection (h/150) showed a minimal effect on the ultimate web-crippling capacity, validating the robustness of an idealized geometry. The research findings underscore that 90° lip stiffeners markedly enhance web-crippling resistance, whereas oblique configurations do not. Finite element analysis has emerged as a powerful design tool capable of reducing reliance on extensive physical testing, refining parametric studies, and guiding more efficient and reliable cold-formed- steel structures.

3. Results

3.1. Analysis of Experimental Results Against Numerical Simulations

This research systematically investigates and compares experimental and numerical outcomes to test the performance of cold-formed steel-lipped Z-sections under ETF and ITF loading conditions. The experimental tests were

conducted on 48 specimens, and the outcomes were compared with FEA predictions to quantify the precision of the numerical model. There was a significant correlation between the deformation modes, stress distribution, and failure modes, which verified the accuracy of FEA in predicting the web-crippling behaviour of cold-formed SFHZ sections.

3.2. Evaluation of Structural Performance

Experimental observations and numerical modelling both determined that CFZ sections possessed reliable material strength, stiffened flanges, and uniform torsional and lateral stability for the end-two-flange and interior-two-flange load cases. The structural response of the sections subjected to load was examined in terms of load-deflection behaviour, stress distribution, and failure modes, with an emphasis on localized web crippling effects. A comparison of the FEA results and experimental results confirmed that the numerical model accurately described the actual mechanical behaviour of the Z-sections.

Additional testing was performed to validate the FEA model, and the numerical predictions were maintained consistently under different loading conditions. This study proves the robustness of FEA in the simulation of CFS behaviour and shows its use in design optimization and structural analysis. The test-to-predicted ratio of the web crippling strength was used as a leading indicator for the evaluation of model accuracy.

3.3. Load-Deflection Behaviour: Experimental vs. FEA Predictions

In general, the experimental and FEA comparisons indicated a good correlation, thereby validating the accuracy of the numerical model. Figure 11 illustrates the comparative analysis between the experimental (EXP) testing failure and FEA simulation failures in a Z_1 (200×55×18×1.2 mm) section concerning the ETF load application. Figure 12 shows that the failure owing to the localized stress concentration is mainly of the web-crippling type. Significant web buckling can be observed in both the experimental and FEA results, particularly in the load-carrying region of the section.

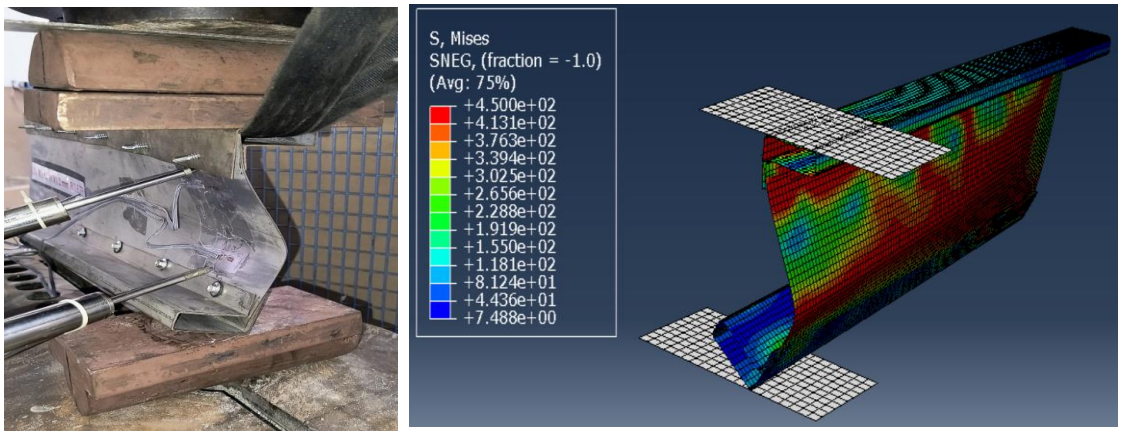

Figure 11. Comparative Study of EXP and FEA Failure Modes in ETF load case

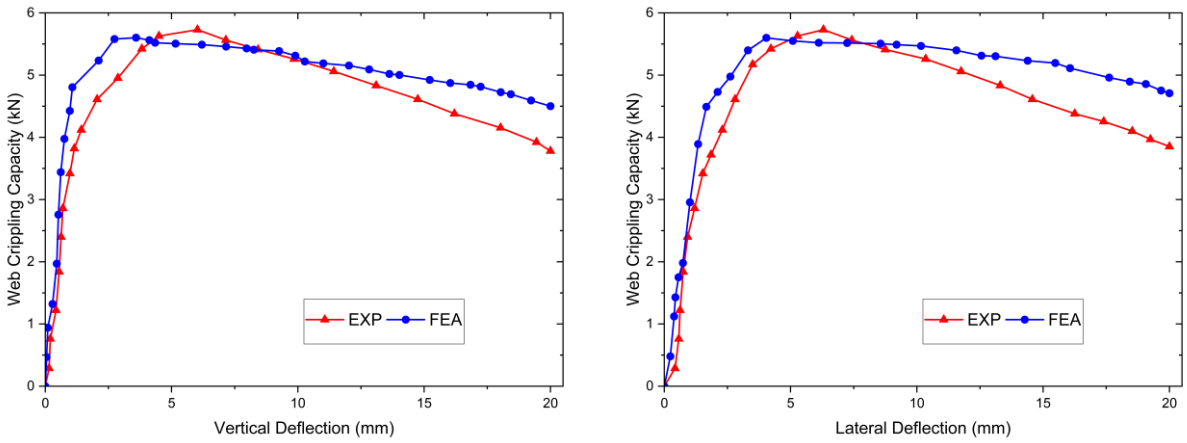

Figure 12. Comparison of load-deformation curves from EXP & FEA for ITF of Z_1

The failure mode of the experiments is in good agreement with the FEA predictions, verifying that the numerical model closely mimics the real behaviour. Any small differences between the experimental and FEA results were likely due to small material property imperfections, geometric irregularities, or differences in the experimental boundary

conditions. However, the similarity in the failure patterns ensured the accuracy of the finite element method for predicting ETF loading responses.

Figure 13 illustrates the failure modes of a Z_2 (150×55×18×1.6 mm) section under Interior-Two-Flange (ITF) loading, contrasting experimental observations with the FEA simulations. Under ITF loading conditions, failure is mainly caused by web buckling and localized web section deformation. The failure mode is different from ETF loading, as ITF specimens undergo more constrained deformation, with the web compressed between the two support plates, resulting in localized stress concentration at the points of load application.

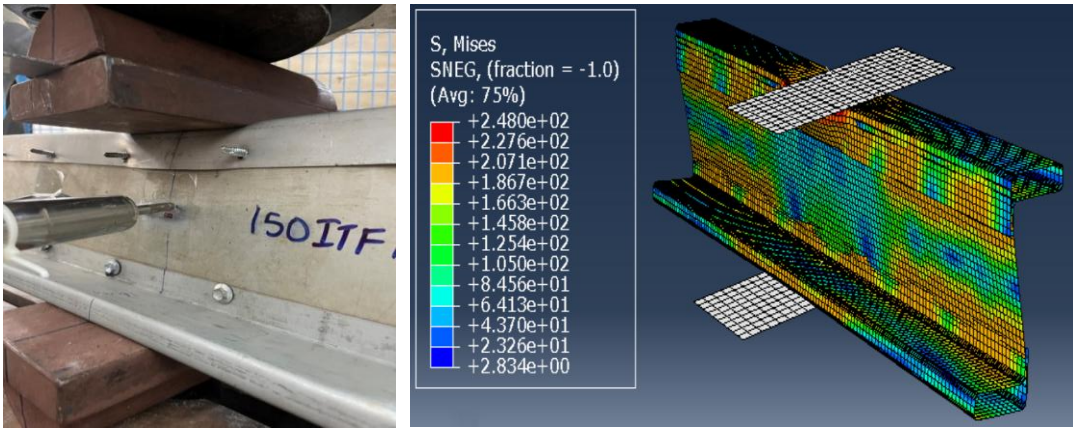

Figure 13. Comparative Study of EXP and FEA Failure Modes in ITF load case

For the ETF load case (Figure 12), the load-deflection curve is linearly elastic up to a deflection of approximately 4 mm, followed by plastic deformation, resulting in an ultimate stress at a deflection of approximately 20 mm. This indicates that the Z-sections under ETF loading exhibit stable elastic behaviour before entering web-crippling failure. For the ITF load case (Figure 14), the elastic range increases to 6 mm of deflection, reflecting a marginally higher initial stiffness than the ETF loading. The ultimate failure is beyond 20 mm of deflection, reflecting that ITF sections can withstand marginally higher deformations before structural failure because of the improved load distribution between the flanges.

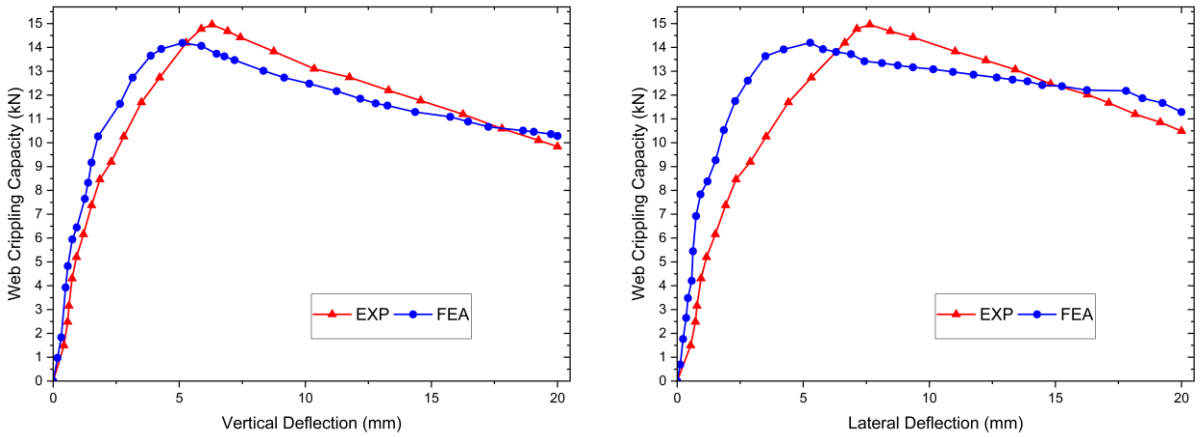

Figure 14. Comparison of load-deformation curves from EXP & FEA for ITF of Z_2

These findings verify that FEA accurately simulates the experimental observations with little variation owing to fabrication tolerances, small geometric imperfections, and material property variations.

Figure 15 effectively depicts the progression of web-crippling failure yield mechanism of various phases: Figure 15(a) showing web-crippling in SFHZ-section begins with an initial phase in the FEA. In pre-ultimate phase shows in the Figure 15(b), the web bucking initiated at the yield stress at 445 MPa near mid-height of the web. As the load further increased, the stress concentration propagated to the nearby section. The ultimate failure phase crippled at elastic stress 450 MPa at 90 increments (Figure 15(c)). Furthermore, the load diminishes due to extensive deformation at post-ultimate phase in Figure 15(d). At this stage, the stress propagated to the entire span which reveals that the section reaches the ultimate stage of failure. The in-depth- parametric study of web-thickness, inner bent radius, and bearing length, to thoroughly examine the web-crippling behaviour under the Z_1-section of ETF loading case.

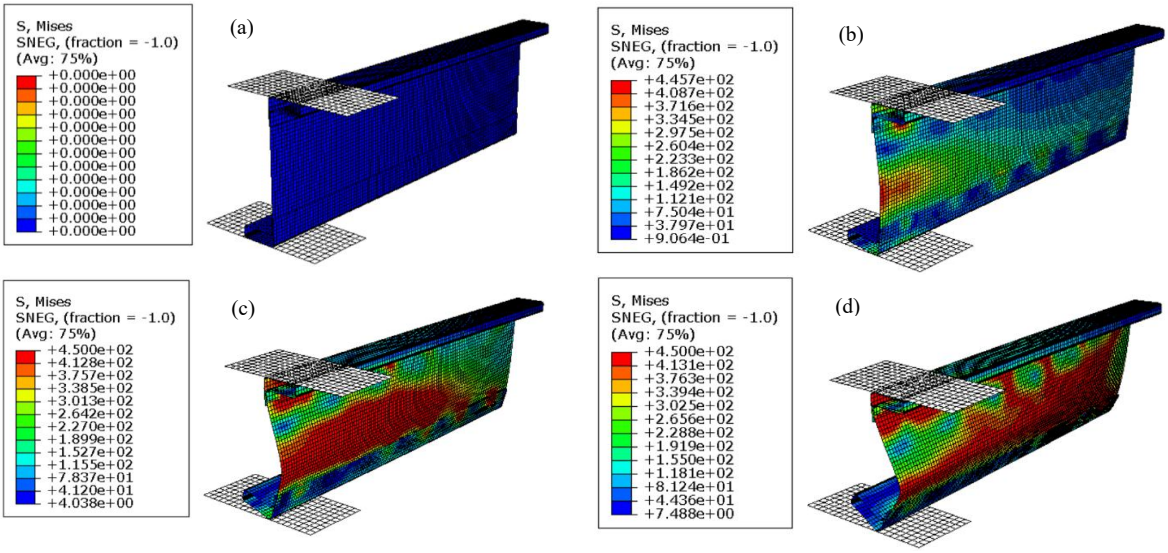

Figure 15. Web-crippling failure yield mechanism of SFHZ-section beam of Z_1 (a) Initial- phase (b) pre-ultimate phase (c) Ultimate-phase (d) Post ultimate-phase

Web crippling in cold-formed steel sections is a localized failure mechanism that occurs under concentrated transverse loads. It initiates with yielding near the web-flange junction, followed by progressive plastic deformation and, depending on web slenderness, may involve local buckling or crushing. The failure culminates in severe out-of-plane deformation and a rapid loss of load capacity. This mechanism is influenced by factors such as geometry, material properties, and boundary conditions, and can be effectively captured through nonlinear finite element analysis.

3.4. Assessment of Web-Crippling Capacities: Experimental and Numerical Insights

The test-to-predicted web-crippling capacity ratios were assessed using the AISI S100 standard, and the results demonstrated the relationships between the experimental and numerical analyses (Tables 4 and 5).

Table 4. Comparative Analysis of Web crippling test & numerical values for ETF

S. No.	$d \times b_f \times d_f \times t_f \times t_w$	f_{yw} (MPa)	r_i (mm)	l_b (mm)	r_i/t	l_b/t	d_1/t	P_{EXP} (kN)	P_{FEA} (kN)	P_{EXP}/P_{FEA}
1	150×55×18×1.2×1.2	457	3	50	2.50	41.66	95.00	4.85	4.68	1.04
2	200×55×18×1.2×1.2	457	3	50	2.50	41.66	136.67	4.52	4.29	1.05
3	150×55×18×1.6×1.6	248	3	50	1.88	31.25	71.25	6.12	5.97	1.03
4	200×55×18×1.6×1.6	248	3	50	1.88	31.25	102.50	5.69	5.51	1.03
5	150×55×18×2.0×2.0	226	3	50	1.50	25.00	57.00	8.82	8.79	1.00
6	200×55×18×2.0×2.0	226	3	50	1.50	25.00	82.00	8.27	8.14	1.02
7	150×55×18×1.2×1.2	457	3	100	2.50	83.33	95.00	6.60	6.12	1.08
8	200×55×18×1.2×1.2	457	3	100	2.50	83.33	136.67	5.73	5.60	1.02
9	150×55×18×1.6×1.6	248	3	100	1.88	62.50	71.25	7.95	7.62	1.04
10	200×55×18×1.6×1.6	248	3	100	1.88	62.50	102.50	7.32	6.95	1.05
11	150×55×18×2.0×2.0	226	3	100	1.50	50.00	57.00	9.64	9.48	1.02
12	200×55×18×2.0×2.0	226	3	100	1.50	50.00	82.00	8.96	8.76	1.02
13	150×55×18×1.2×1.2	457	4	50	3.33	41.66	95.00	4.57	4.29	1.07
14	200×55×18×1.2×1.2	457	4	50	3.33	41.66	136.67	4.18	3.74	1.12
15	150×55×18×1.6×1.6	248	4	50	2.50	31.25	71.25	5.84	5.48	1.06
16	200×55×18×1.6×1.6	248	4	50	2.50	31.25	102.50	5.34	4.81	1.11
17	150×55×18×2.0×2.0	226	4	50	2.00	25.00	57.00	8.16	8.48	0.96
18	200×55×18×2.0×2.0	226	4	50	2.00	25.00	82.00	7.98	7.96	1.00
19	150×55×18×1.2×1.2	457	4	100	3.33	83.33	95.00	5.19	4.74	1.09
20	200×55×18×1.2×1.2	457	4	100	3.33	83.33	136.67	4.82	4.46	1.08
21	150×55×18×1.6×1.6	248	4	100	2.50	62.50	71.25	6.97	6.59	1.06
22	200×55×18×1.6×1.6	248	4	100	2.50	62.50	102.50	5.97	5.64	1.06
23	150×55×18×2.0×2.0	226	4	100	2.00	50.00	57.00	9.15	8.78	1.04
24	200×55×18×2.0×2.0	226	4	100	2.00	50.00	82.00	8.50	8.28	1.03
									Mean	**1.05**
									COV	**0.03**

Table 5. Comparative Analysis of web crippling test & numerical values for ITF

S. No.	$d \times b_f \times d_f \times t_f \times t_w$	f_{yw} (MPa)	r_i	l_b (mm)	r_i/t	l_b/t	d_1/t	P_{EXP} (kN)	P_{FEA} (kN)	P_{EXP}/P_{FEA}
1	150×55×18×1.2×1.2	457	3	50	2.50	41.66	95.00	9.62	9.18	1.05
2	200×55×18×1.2×1.2	457	3	50	2.50	41.66	136.67	9.02	8.97	1.00
3	150×55×18×1.6×1.6	248	3	50	1.88	31.25	71.25	11.98	11.24	1.07
4	200×55×18×1.6×1.6	248	3	50	1.88	31.25	102.50	11.02	10.65	1.03
5	150×55×18×2.0×2.0	226	3	50	1.50	25.00	57.00	16.80	16.29	1.03
6	200×55×18×2.0×2.0	226	3	50	1.50	25.00	82.00	16.48	16.18	1.02
7	150×55×18×1.2×1.2	457	3	100	2.50	83.33	95.00	10.81	10.68	1.01
8	200×55×18×1.2×1.2	457	3	100	2.50	83.33	136.67	10.17	9.92	1.03
9	150×55×18×1.6×1.6	248	3	100	1.88	62.50	71.25	14.96	14.19	1.05
10	200×55×18×1.6×1.6	248	3	100	1.88	62.50	102.50	13.54	13.18	1.03
11	150×55×18×2.0×2.0	226	3	100	1.50	50.00	57.00	20.17	19.83	1.02
12	200×55×18×2.0×2.0	226	3	100	1.50	50.00	82.00	19.26	18.92	1.02
13	150×55×18×1.2×1.2	457	4	50	3.33	41.66	95.00	7.85	7.17	1.09
14	200×55×18×1.2×1.2	457	4	50	3.33	41.66	136.67	7.63	6.98	1.09
15	150×55×18×1.6×1.6	248	4	50	2.50	31.25	71.25	10.83	10.39	1.04
16	200×55×18×1.6×1.6	248	4	50	2.50	31.25	102.50	10.09	9.96	1.01
17	150×55×18×2.0×2.0	226	4	50	2.00	25.00	57.00	15.19	15.02	1.01
18	200×55×18×2.0×2.0	226	4	50	2.00	25.00	82.00	14.86	14.37	1.03
19	150×55×18×1.2×1.2	457	4	100	3.33	83.33	95.00	9.98	9.73	1.03
20	200×55×18×1.2×1.2	457	4	100	3.33	83.33	136.67	9.48	9.13	1.04
21	150×55×18×1.6×1.6	248	4	100	2.50	62.50	71.25	12.57	12.38	1.02
22	200×55×18×1.6×1.6	248	4	100	2.50	62.50	102.50	11.86	11.53	1.03
23	150×55×18×2.0×2.0	226	4	100	2.00	50.00	57.00	18.92	18.16	1.04
24	200×55×18×2.0×2.0	226	4	100	2.00	50.00	82.00	18.19	17.69	1.03
									Mean	**1.03**
									COV	**0.02**

These results suggest that the current AISI S100 specifications are unconservative, particularly in the case of screw-fastened hollow Z-sections, because the test data consistently exceeded the predictions based on the standard equations. The new FEA model provided a better picture of the load-bearing behaviour than the standard design calculations.

3.5. Implications for Code Improvement and Structural Design

The implications of this comparative study for the design and analysis of cold-formed steel Z-sections are significant.

- The present AISI S100 predictions are conservative for hollow Z-sections fastened with screws, which results in overestimation of the web-crippling strength.
- Finite Element Analysis (FEA) is a better structural analysis tool with improved precision for predicting stress patterns and failure modes compared to conventional design formulas.
- Load-deflection behaviour validates that ITF sections are more resistant to web crippling than ETF sections, and thus they are ideal for use in applications requiring higher load-bearing capacity.
- An updated web-crippling coefficient update using experimental and FEA data can potentially enhance the design precision and structural reliability.
- These findings confirm the value of numerical modelling for enhancing cold-formed steel designs to minimize physical testing and increase engineering standards for predicting structural performance

4. Proposed Equation for Screw-Fastened Capacity in Z-Section

AISI web crippling coefficients were calibrated based on 240 parametric analyses conducted using finite element (FE) models. The analyses involved varying several significant parameters: elastic limit (226 to 457 MPa), web thickness (1.2, 1.6, and 2.0 mm), corner radius (3 and 4 mm), bearing length (50 and 100 mm), and section depth (150 and 200

mm). The output from such FE models was interpreted using nonlinear regression techniques and placed in the frame of the design formulation as per AISI standards.

Moreover, the reduction factor of the capacity was calculated using Equation 4 for AISI S100 and AS/NZS 4600. The revised coefficients enhance the web-crippling predictions of cold-formed screw-fastened Z-sections under the ETF and ITF load cases in Equation 5. The coefficients may be used for the AISI web crippling equations for any standard sample size. The reliability-based equation suggested in this study includes variations in the material properties, fabrication quality, experimental outcomes, and effects of loading, as represented by the following parameters:

The capacity reduction factor (Φ_w) is defined as follows:

$$\Phi_w = \mathrm{C}_\Phi \mathrm{M}_m \mathrm{F}_m \mathrm{P}_m e^{-\beta_0 \sqrt{V_M{}^2 + V_F{}^2 + C_P V_P{}^2 + V_Q{}^2}} \quad (4)$$

where, $\mathrm{V_M}$, V_F, V_P, and V_Q - COV for Characteristics of materials, manufacturing techniques, experimental observations, and effects of loading and M_m, F_m, and P_m Mean values for variations in material, fabrication, and professional factors, $C\Phi$ - Calibration efficiency factor, C_P - Correction factor, βo - Reliability index:

The proposed web-crippling capacity equation for screw-fastened Z-sections is given as:

$$P_p = C t_w^2 f_{yw} \sin\theta \left(1 - C_h \sqrt{\frac{d_1}{t_w}}\right)\left(1 - C_{ri}\sqrt{\frac{r_i}{t_w}}\right)\left(1 + C_{lb}\sqrt{\frac{l_b}{t_w}}\right) \quad (5)$$

4.1. Validation of Proposed Equation

In the case of the ETF load case, the mean ratio of test-to-predicted web crippling capacity was 1.61, with a coefficient of variation (COV) of 0.10, as evident in Table 6. ITF load case, the mean test-to-predicted web crippling capacity was 1.60 and the COV was 0.18, as depicted in Table 7.

Table 6. Comparative Analysis of Web Crippling Capacity CFSFHZ and FEA for ETF

S. No.	d×b$_f$×d$_f$×t$_f$×t$_w$	f$_{yw}$ (MPa)	r$_i$/t	l$_b$/t	d$_1$/t	P$_{EXP}$ (kN)	P$_{FEA}$ (kN)	P$_{EXP}$ /P$_{FEA}$	P$_{AISI}$ (kN)	P$_{EXP}$ /P$_{AISI}$
1	150×55×18×1.2×1.2	457	2.50	41.66	95.00	4.85	4.68	1.04	3.41	1.42
2	200×55×18×1.2×1.2	457	2.50	41.66	136.67	4.52	4.29	1.05	2.98	1.52
3	150×55×18×1.6×1.6	248	1.88	31.25	71.25	6.12	5.97	1.03	3.93	1.56
4	200×55×18×1.6×1.6	248	1.88	31.25	102.50	5.69	5.51	1.03	3.53	1.61
5	150×55×18×2.0×2.0	226	1.50	25.00	57.00	8.82	8.79	1.00	6.24	1.41
6	200×55×18×2.0×2.0	226	1.50	25.00	82.00	8.27	8.14	1.02	5.70	1.45
7	150×55×18×1.2×1.2	457	2.50	83.33	95.00	6.60	6.12	1.08	3.76	1.76
8	200×55×18×1.2×1.2	457	2.50	83.33	136.67	5.73	5.60	1.02	3.28	1.75
9	150×55×18×1.6×1.6	248	1.88	62.50	71.25	7.95	7.62	1.04	4.29	1.85
10	200×55×18×1.6×1.6	248	1.88	62.50	102.50	7.32	6.95	1.05	3.85	1.90
11	150×55×18×2.0×2.0	226	1.50	50.00	57.00	9.64	9.48	1.02	6.75	1.43
12	200×55×18×2.0×2.0	226	1.50	50.00	82.00	8.96	8.76	1.02	6.17	1.45
13	150×55×18×1.2×1.2	457	3.33	41.66	95.00	4.57	4.29	1.07	N. A	
14	200×55×18×1.2×1.2	457	3.33	41.66	136.67	4.18	3.74	1.12	N. A	
15	150×55×18×1.6×1.6	248	2.50	31.25	71.25	5.84	5.48	1.06	3.46	1.69
16	200×55×18×1.6×1.6	248	2.50	31.25	102.50	5.34	4.81	1.11	3.10	1.72
17	150×55×18×2.0×2.0	226	2.00	25.00	57.00	8.16	8.48	0.96	5.61	1.45
18	200×55×18×2.0×2.0	226	2.00	25.00	82.00	7.98	7.96	1.00	5.13	1.56
19	150×55×18×1.2×1.2	457	3.33	83.33	95.00	5.19	4.74	1.09	N. A	
20	200×55×18×1.2×1.2	457	3.33	83.33	136.67	4.82	4.46	1.08	N. A	
21	150×55×18×1.6×1.6	248	2.50	62.50	71.25	6.97	6.59	1.06	3.77	1.85
22	200×55×18×1.6×1.6	248	2.50	62.50	102.50	5.97	5.64	1.06	3.39	1.76
23	150×55×18×2.0×2.0	226	2.00	50.00	57.00	9.15	8.78	1.04	6.08	1.51
24	200×55×18×2.0×2.0	226	2.00	50.00	82.00	8.50	8.28	1.03	5.55	1.53
							Mean	**1.05**		**1.61**
							COV	**0.03**		**0.10**

Note: N.A.- AISI formulation is inapplicable for $r_i/t \leq 3$.

Table 7. Comparative Analysis of Web Crippling Capacity CFSFHZ and FEA for ITF

S. No.	$d \times b_f \times d_f \times t_f \times t_w$	f_{yw} (MPa)	r_i/t	l_b/t	d_1/t	P_{EXP} (kN)	P_{FEA} (kN)	P_{EXP}/P_{FEA}	P_{AISI} (kN)	P_{EXP}/P_{AISI}
1	150×55×18×1.2×1.2	457	2.50	41.66	95.00	9.62	9.18	1.05	5.47	1.76
2	200×55×18×1.2×1.2	457	2.50	41.66	136.67	9.02	8.97	1.00	5.46	1.65
3	150×55×18×1.6×1.6	248	1.88	31.25	71.25	11.98	11.24	1.07	8.00	1.50
4	200×55×18×1.6×1.6	248	1.88	31.25	102.50	11.02	10.65	1.03	7.99	1.38
5	150×55×18×2.0×2.0	226	1.50	25.00	57.00	16.80	16.29	1.03	13.68	1.23
6	200×55×18×2.0×2.0	226	1.50	25.00	82.00	16.48	16.18	1.02	13.66	1.21
7	150×55×18×1.2×1.2	457	2.50	83.33	95.00	10.81	10.68	1.01	6.59	1.64
8	200×55×18×1.2×1.2	457	2.50	83.33	136.67	10.17	9.92	1.03	6.58	1.55
9	150×55×18×1.6×1.6	248	1.88	62.50	71.25	14.96	14.19	1.05	9.51	1.57
10	200×55×18×1.6×1.6	248	1.88	62.50	102.50	13.54	13.18	1.03	9.49	1.43
11	150×55×18×2.0×2.0	226	1.50	50.00	57.00	20.17	19.83	1.02	16.11	1.25
12	200×55×18×2.0×2.0	226	1.50	50.00	82.00	19.26	18.92	1.02	16.09	1.20
13	150×55×18×1.2×1.2	457	3.33	41.66	95.00	7.85	7.17	1.09	N. A	
14	200×55×18×1.2×1.2	457	3.33	41.66	136.67	7.63	6.98	1.09	N. A	
15	150×55×18×1.6×1.6	248	2.50	31.25	71.25	10.83	10.39	1.04	4.94	2.19
16	200×55×18×1.6×1.6	248	2.50	31.25	102.50	10.09	9.96	1.01	4.93	2.05
17	150×55×18×2.0×2.0	226	2.00	25.00	57.00	15.19	15.02	1.01	9.97	1.52
18	200×55×18×2.0×2.0	226	2.00	25.00	82.00	14.86	14.37	1.03	9.96	1.49
19	150×55×18×1.2×1.2	457	3.33	83.33	95.00	9.98	9.73	1.03	N. A	
20	200×55×18×1.2×1.2	457	3.33	83.33	136.67	9.48	9.13	1.04	N. A	
21	150×55×18×1.6×1.6	248	2.50	62.50	71.25	12.57	12.38	1.02	5.87	2.14
22	200×55×18×1.6×1.6	248	2.50	62.50	102.50	11.86	11.53	1.03	5.86	2.02
23	150×55×18×2.0×2.0	226	2.00	50.00	57.00	18.92	18.16	1.04	11.74	1.61
24	200×55×18×2.0×2.0	226	2.00	50.00	82.00	18.19	17.69	1.03	11.72	1.55
							Mean	**1.03**		**1.60**
							COV	**0.02**		**0.18**

Note: N.A.- AISI formulation is inapplicable for $r_i/t \leq 3$.

The Table 8 compares experimental, FEA, and proposed equation-based web-crippling capacities for ETF and ITF load scenarios. The result shows the proposed coefficients offer dramatic improvements in accuracy compared to the AISI S100 design equations. A comparison of the test-to-predicted ratios further supported the effectiveness of the proposed equation in assessing the web crippling capacities under ETF and ITF load cases. The proposed equation demonstrates appreciable improvement in accuracy and uniformity in comparison to AISI S100 predictions. In the ETF load case, the AISI S100 method overestimates the strength extensively with a mean ratio of 1.61 and a coefficient of variation (COV) of 0.08. Contrarily, the proposed equation provides a much more accurate prediction with a mean ratio of 1.04, having a COV of 0.08, depicting less variability and more consistency in the results.

Similarly, in the ITF load case, the AISI S100 method continues with overestimation with a mean ratio of 1.60, while the proposed equation provides a better mean ratio of 1.02, having a COV of 0.09. These findings demonstrate that the proposed equation yields more accurate web-crippling strength predictions, eliminating overestimation problems in current design standards.

Table 8. Comparative evaluation of web-crippling capacity: CFSFHZ, FEA and Proposed analytical coefficients for ETF and ITF

S. No.	Screw-fastened Hollow Z-section Beam ($d \times b_f \times d_f \times t_f \times t_w$)	ETF			ITF		
		P_{EXP}	P_{EXP}/P_{AISI}	P_{FEA}/P_{AISI}	P_{EXP}	P_{EXP}/P_{AISI}	P_{FEA}/P_{AISI}
1	150×55×18×1.2×1.2	4.85	0.85	0.83	9.62	0.87	0.83
2	200×55×18×1.2×1.2	4.52	0.88	0.83	9.02	0.90	0.89
3	150×55×18×1.6×1.6	6.12	1.09	1.06	11.98	1.09	1.02
4	200×55×18×1.6×1.6	5.69	1.09	1.06	11.02	1.08	1.04
5	150×55×18×2.0×2.0	8.82	1.09	1.08	16.80	1.05	1.02
6	200×55×18×2.0×2.0	8.27	1.09	1.07	16.48	1.10	1.08
7	150×55×18×1.2×1.2	6.60	0.98	0.91	10.81	0.83	0.82
8	200×55×18×1.2×1.2	5.73	0.93	0.91	10.17	0.85	0.83
9	150×55×18×1.6×1.6	7.95	1.20	1.16	14.96	1.16	1.10
10	200×55×18×1.6×1.6	7.32	1.20	1.14	13.54	1.13	1.10
11	150×55×18×2.0×2.0	9.64	1.02	1.01	20.17	1.09	1.07
12	200×55×18×2.0×2.0	8.96	1.02	0.99	19.26	1.11	1.09
13	150×55×18×1.2×1.2	4.57	N. A		7.85	N. A	
14	200×55×18×1.2×1.2	4.18	N. A		7.63	N. A	
15	150×55×18×1.6×1.6	5.84	1.07	1.01	10.83	1.03	0.98
16	200×55×18×1.6×1.6	5.34	1.06	0.95	10.09	1.03	1.02
17	150×55×18×2.0×2.0	8.16	1.03	1.07	15.19	0.99	0.98
18	200×55×18×2.0×2.0	7.98	1.08	1.08	14.86	1.03	0.99
19	150×55×18×1.2×1.2	5.19	N. A		9.98	N. A	
20	200×55×18×1.2×1.2	4.82	N. A		9.48	N. A	
21	150×55×18×1.6×1.6	6.97	1.09	1.03	12.57	1.01	1.00
22	200×55×18×1.6×1.6	5.97	1.01	0.95	11.86	1.03	1.00
23	150×55×18×2.0×2.0	9.15	1.00	0.96	18.92	1.06	1.01
24	200×55×18×2.0×2.0	8.50	0.99	0.96	18.19	1.08	1.05
		Mean	**1.04**	**1.00**		**1.02**	**1.00**
		COV	**0.08**	**0.09**		**0.09**	**0.09**

4.2. Recommended Web-Crippling Coefficients for CFSFHZ-sections

The revised web-crippling coefficients for the ETF and ITF loads were compared with those for the ETF and ITF loads, and the AISI S100 standards were compared with the newly proposed values in Table 9.

Table 6. Proposed web-crippling coefficients of ETF & ITF loads

Load case	Coefficients	C	C_r	C_{lb}	C_w	Φ_w	Mean	COV
ETF	AISI	13	0.32	0.05	0.04	0.90	1.61	0.10
	Proposed	8.4	0.12	0.13	0.032	0.89	1.04	0.08
ITF	AISI	24	0.52	0.15	0.001	0.80	1.60	0.18
	Proposed	17.1	0.15	0.13	0.031	0.80	1.02	0.09

This study investigates the web-crippling behaviour of an unfastened CFSFHZ for resisting ETF and ITF loading scenarios. A comprehensive approach combining experimental testing, FEA, and parametric investigation was adopted to analyse the structural behaviour of such sections. The web-crippling capacity was tested for 48 specimens and compared against American and AS/NZS design code predictions. The comparison revealed that both standards provided conservative strength estimates for sections with an internal bend radius to material thickness ratio ($\frac{r_i}{t}$) up to 3.3, but became excessively conservative beyond this threshold. The same applied to lipped Z-sections, in which forecasts were conservative for a lip-to-thickness ($\frac{l_b}{t}$) ratio of as much as 84 but were too conservative for any value beyond this, particularly for edge ETF and ITF configurations.

The AISI-S100 and existing methods tend to underestimate web crippling strength by up to 18%, whereas the proposed coefficients reduce the prediction error to within 3%. While the current methodology relies on empirical equations based on past experiments, the proposed approach uses regression-based coefficients derived from finite element analysis and experimental data. For thin web effects in the web, existing procedures are conservative, particularly for high slenderness ratios, whereas the proposed method provides more accurate results in slender web section situations. Existing procedures have limited validation when applied to new cold-formed steel (CFS) profiles, and the proposed coefficients have been calibrated through extensive testing and full-scale FEA. Lastly, the safety factors in existing methods may be overly conservative, but the proposed approach adjusts these factors to more accurately reflect experimental results.

5. Conclusion

The proposed study and comprehensive evaluation of combined experimental testing and nonlinear finite element analysis to probe the web-crippling performance of cold-formed, screw-fastened hollow sections under End-Two-Flange (ETF) and Interior-Two-Flange (ITF) loading scenarios. 48 specimens, with varying material thicknesses, bearing lengths, and inner bent radius, were methodically evaluated to separate the effect of each geometric parameter on failure mechanisms and web-crippling strength. Whereas tighter inner bent radius increases stress concentrations and precipitates earlier web-crippling failures, parametric study showed that increases in web thickness and extended bearing lengths greatly increase the load-carrying capacity. Consistent conservatism in the current design equations revealed by comparative benchmarking against the AISI S100 and AS/NZS 4600 requirements suggests the possibility for material overdesign. Parametric studies of general nature were applied to develop novel calibrated coefficients and proposed equations. The stability of the revised equations for effectiveness was demonstrated through reliability-based validation with a demonstration of 15% mean reduction of design conservatism for a coefficient of variation of less than 0.10. By enabling improved estimation of web crippling capacity, these expressions invite maximum material usage without compromising on structural integrity. The conclusions reached in the work form a basis for updating specifications for design requirements of cold-formed steel and design inclusion of screw-fastened Z section beams within lightweight structural frames. These coefficients can be made part of structural design software with a view to optimizing processes and delivering measurable resource and construction costs savings. In addition, deeper exploration of the residual stress effects and manufacturing variability promises to enhance the further improvement in the model fidelity and predictability.

6. Notations

d	Overall depth	d_1	Clear web heights
b_f	Flange breadth	t_w	Web thickness
t_f	Flange gauge	f_{yw}	Yield stresses
l_b	Loading plate length	C_{lb}	Loading length coefficient
r_i	Inner bent radius	Cr_i	Inner bent radius coefficient
C_W	Web height coefficient	C	Coefficient
P_n	Web-crippling strength	θ	Web-to-surface angle
E	Modulus of elasticity	f_u	Critical fracture stress
ε_u	Gauge length		

7. Declarations

7.1. Author Contributions

Conceptualization, K.S. and J.A.V.; methodology, K.S. and J.A.V.; software, K.S.; validation, K.S. and J.A.V.; formal analysis, K.S.; investigation, K.S.; resources, K.S.; data curation, K.S. and J.A.V.; writing—original draft preparation, K.S.; writing—review and editing, K.S. and J.A.V.; visualization, K.S.; supervision, J.A.V.; project administration, J.A.V.; funding acquisition, J.A.V. All authors have read and agreed to the published version of the manuscript.

7.2. Data Availability Statement

The data presented in this study are available on request from the corresponding author.

7.3. Funding

We would like to thank the management of Vellore Institute of Technology (VIT) for providing open access fund for publication of this article.

7.4. Conflicts of Interest

The authors declare no conflict of interest.

8. References

[1] Meza, F. J., Becque, J., & Hajirasouliha, I. (2020). Experimental study of cold-formed steel built-up columns. Thin-Walled Structures, 149, 106291. doi:10.1016/j.tws.2019.106291.

[2] N.Usefi, Sharafi, P., Mortazavi, M., Ronagh, H., & Samali, B. (2021). Structural performance and sustainability assessment of hybrid-cold formed modular steel frame. Journal of Building Engineering, 34, 101895. doi:10.1016/j.jobe.2020.101895.

[3] Thirunavukkarasu, K., Kanthasamy, E., Gatheeshgar, P., Poologanathan, K., Rajanayagam, H., Suntharalingam, T., & Dissanayake, M. (2021). Sustainable performance of a modular building system made of built-up cold-formed steel beams. Buildings, 11(10), 460. doi:10.3390/buildings11100460.

[4] Winter, G., & Pian, R. H. J. (1946). Crushing strength of thin steel webs. Cornell Bulletin, 35, 1-24.

[5] AISI S100-16. (2016). North American Specification for the Design of Cold-Formed Steel Structural Members. American Iron and Steel Institute (AISI), Washington, United States.

[6] AS/NZS 4600. (2018). Australian / New Zealand Standard TM Cold-formed steel structures. Standard Australia, Sydney, Australia.

[7] S136-94. (1994). Cold Formed Steel Structural Members. Canadian Standards Association, Toronto, Canada.

[8] Hetrakul, N., & Yu, W. W. (1978). Structural behavior of beam webs subjected to web crippling and a combination of web crippling and bending. Final Report, Civil Engineering Study, University of Missouri-Rolla, Rolla, United States.

[9] Santaputra, C. (1986). Web crippling of high strength cold-formed steel beams. Ph.D. Thesis, University of Missouri-Rolla, Rolla, United States.

[10] Bhakta, B. H., LaBoube, R. A., & Yu, W. W. (1992). The effect of flange restraint on web crippling strength. Technical Report, Missouri University of Science and Technology, Rolla, United States.

[11] Janarthanan, B., Mahendran, M., & Gunalan, S. (2019). Numerical modelling of web crippling failures in cold-formed steel unlipped channel sections. Journal of Constructional Steel Research, 158, 486–501. doi:10.1016/j.jcsr.2019.04.007.

[12] Janarthanan, B., & Mahendran, M. (2020). Numerical study of cold-formed steel channel sections under combined web crippling and bending action. Thin-Walled Structures, 152, 106766. doi:10.1016/j.tws.2020.106766.

[13] Kanthasamy, E., Chandramohan, D. L., Shanmuganathan, G., Poologanathan, K., Gatheeshgar, P., Corradi, M., & Mcintosh, A. (2022). Web crippling behaviour of cold-formed high-strength steel unlipped channel beams under End-One-Flange load case. Case Studies in Construction Materials, 16. doi:10.1016/j.cscm.2022.e01022.

[14] Young, B., Ellobody, E., & He, J. (2023). Web crippling tests on cold-formed high strength steel channel sections having different stiffened flanges and stiffened web. Thin-Walled Structures, 190, 110995. doi:10.1016/j.tws.2023.110995.

[15] Lan, X., Zhang, J. J., & Zhao, O. (2024). High strength steel unlipped channel sections subjected to ETF loading: Laboratory testing, numerical simulations and web crippling design. Engineering Structures, 319, 118852. doi:10.1016/j.engstruct.2024.118852.

[16] He, J., & Ellobody, E. (2024). Nonlinear web crippling analysis and design of cold-formed high strength steel channel sections having different stiffened flanges. Thin-Walled Structures, 197, 111651. doi:10.1016/j.tws.2024.111651.

[17] Prabaharan, V., & Akhas, P. K. (2025). Evaluating the influence of stiffener in the bending capacity of cold formed steel C-section. Innovative Infrastructure Solutions, 10(3), 118. doi:10.1007/s41062-025-01914-1.

[18] McIntosh, A., Kanthasamy, E., Poologanathan, K., Gunalan, S., Gatheeshgar, P., Corradi, M., & Higgins, C. (2022). Web crippling design of channel beams: Carbon steel, stainless steel and aluminium. Journal of Constructional Steel Research, 196, 107427. doi:10.1016/j.jcsr.2022.107427.

[19] Chen, B., Roy, K., Fang, Z., Uzzaman, A., Chi, Y., & Lim, J. B. P. (2021). Web crippling capacity of fastened cold-formed steel channels with edge-stiffened web holes, un-stiffened web holes and plain webs under two-flange loading. Thin-Walled Structures, 163, 107666. doi:10.1016/j.tws.2021.107666.

[20] Alsanat, H., Gunalan, S., Poologanathan, K., & Guan, H. (2021). Web crippling investigations of aluminium lipped channel sections under one-flange loading conditions. Thin-Walled Structures, 166, 108025. doi:10.1016/j.tws.2021.108025.

[21] Sundararajah, L., Mahendran, M., & Keerthan, P. (2019). Numerical Modeling and Design of Lipped Channel Beams Subject to Web Crippling under One-Flange Load Cases. Journal of Structural Engineering, 145(10). doi:10.1061/(asce)st.1943-541x.0002367.

[22] Badawy Abu-Sena, A. B., Abdelfattah, F. A., Soliman, M. S., & Saleh, M. S. R. (2020). An experimentally verified new approach for web crippling design of cold-formed steel Z-Sections. Journal of Constructional Steel Research, 164, 105813. doi:10.1016/j.jcsr.2019.105813.

[23] Young, B., & Ellobody, E. (2023). Experimental investigation on cold-formed steel Z-sections having different stiffened flanges undergoing web crippling. Engineering Structures, 286, 116144. doi:10.1016/j.engstruct.2023.116144.

[24] Siva, K., & Visuvasam, J. (2024). An Optimally Designed Cold-Formed Steel Beam Thickness Selection for Reducing Web-Crippling Smartly. International Journal of Steel Structures, 24(3), 515–528. doi:10.1007/s13296-024-00833-8.

[25] Schuster, R. M., & Beshara, B. (2000). Web crippling data and calibrations of cold formed steel members. American Iron and Steel Institute (AISI), Washington, United States.

[26] Holesapple, M. W., & LaBoube, R. A. (2003). Web crippling of cold-formed steel beams at end supports. Engineering Structures, 25(9), 1211–1216. doi:10.1016/S0141-0296(03)00076-2.

[27] Choy, M. Y., Jia, X. F., Yuan, X., Zhou, J., Wang, H. S., & Yu, C. (2014). Direct strength method for web crippling of cold-formed steel C- And Z- sections subjected to two-flange loading. Structural Stability Research Council Annual Stability Conference 2014, SSRC 2014, 99–111.

[28] Zhou, F., Chhun, N., & Cai, Y. (2023). Numerical investigation and design of cold-formed lean duplex stainless steel Z-sections undergoing web crippling. Thin-Walled Structures, 183, 110324. doi:10.1016/j.tws.2022.110324.

[29] Dwivedi, R., & Vyavahare, A. Y. (2023). Numerical Investigation into Web Crippling of Cold-Formed Lipped Z-sections under Two-Flange Loadings. International Journal of Steel Structures, 23(3), 627–644. doi:10.1007/s13296-023-00717-3.

[30] Misiek, T., & Belica, A. (2019). Calibration of European web-crippling equations for cold-formed C- and Z-sections. Steel Construction, 12(1), 31–43. doi:10.1002/stco.201800006.

[31] Dara, M. (2015). Direct Strength Method for Web Crippling of Cold-formed Steel C- and Zsections Subjected to One-flange Loading Martin Dara. Journal of Steel Structures & Construction, 1(1), 4. doi:10.4172/2472-0437.1000105.

[32] Siva, K., Visuvasam, J., & Srikanth, D. (2025). Review of Cold-Formed Steel Z-Section Beams: Design Approaches and Performance Analysis. Structural Design of Tall and Special Buildings, 34(2), e2212. doi:10.1002/tal.2212.

[33] Bock, M., & Real, E. (2014). Strength curves for web crippling design of cold-formed stainless steel hat sections. Thin-Walled Structures, 85, 93–105. doi:10.1016/j.tws.2014.07.021.

[34] Chen, Z., Pham, C. H., & Hancock, G. J. (2025). Plastic mechanism models for use in DSM localised loading design of hat sections. Thin-Walled Structures, 206, 112683. doi:10.1016/j.tws.2024.112683.

[35] Jing, Y., Jiang, K., Zhao, O., & Gardner, L. (2024). Web crippling of stainless steel built-up I-sections under End-Two-Flange loading: Tests, simulations and design. Engineering Structures, 304, 117576. doi:10.1016/j.engstruct.2024.117576.

[36] Martins, A. D., Teixeira, Â. P., Silvestre, N., & Correia, J. R. (2025). Reliability-Based Code Calibration of Pultruded Glass Fibre-Reinforced Polymer I-Section Beams Under End-Two-Flange and Interior-Two-Flange Web-Crippling Loading Cases. Engineerin, 1-37. doi:10.1016/j.eng.2025.03.019.

[37] Put, B. M., Pi, Y.-L., & Trahair, N. S. (1999). Lateral Buckling Tests on Cold-Formed Channel Beams. Journal of Structural Engineering, 125(5), 532–539. doi:10.1061/(asce)0733-9445(1999)125:5(532).

[38] Sundararajah, L., Mahendran, M., & Keerthan, P. (2018). Design of SupaCee Sections Subject to Web Crippling under One-Flange Load Cases. Journal of Structural Engineering, 144(12), 04018222. doi:10.1061/(asce)st.1943-541x.0002206.

[39] Ye, J., Hajirasouliha, I., Becque, J., & Eslami, A. (2016). Optimum design of cold-formed steel beams using Particle Swarm Optimisation method. Journal of Constructional Steel Research, 122, 80–93. doi:10.1016/j.jcsr.2016.02.014.

[40] Gatheeshgar, P., Poologanathan, K., Gunalan, S., Shyha, I., Tsavdaridis, K. D., & Corradi, M. (2020). Optimal design of cold-formed steel lipped channel beams: Combined bending, shear, and web crippling. Structures, 28, 825–836. doi:10.1016/j.istruc.2020.09.027.

[41] Hussein, A. B., & Hussein, D. B. (2024). Effects of Lip Length and Inside Radius-to-Thickness Ratio on Buckling Behavior of Cold-Formed Steel C-Sections. Buildings, 14(3), 587. doi:10.3390/buildings14030587.

[42] Hussein, D. B., & Hussein, A. B. (2024). Investigating the Factors Influencing the Strength of Cold-Formed Steel (CFS) Sections. Buildings, 14(4), 1127. doi:10.3390/buildings14041127.

[43] Dwivedi, R., & Vyavahare, A. Y. (2023). Experimental investigation on cold-formed Z-sections under two-flange loadings. Engineering Structures, 297, 116974. doi:10.1016/j.engstruct.2023.116974.

[44] Taimur, M. A., Ahmad, J., Shakeel, S., & Usman, M. (2024). Effect of web holes on web crippling capacity of rectangular hollow steel sections under two flange loadings. Journal of Constructional Steel Research, 222, 108985. doi:10.1016/j.jcsr.2024.108985.

[45] Yun, X., Meng, X., & Gardner, L. (2022). Design of cold-formed steel SHS and RHS beam–columns considering the influence of steel grade. Thin-Walled Structures, 171. doi:10.1016/j.tws.2021.108600.

[46] Thirunavukkarasu, K., Kanthasamy, E., Pologanathan, K., Gunalan, S., Gatheeshgar, P., Tsavdaridis, K. D., & Corradi, M. (2023). Flexural behaviour and design rules for SupaCee sections with web openings. Journal of Building Engineering, 63. doi:10.1016/j.jobe.2022.105539.

[47] Lalvani, H., & Mandal, P. (2021). Cold forming of Al-5251 and Al-6082 tailored welded blanks manufactured by laser and electron beam welding. Journal of Manufacturing Processes, 68, 1615–1636. doi:10.1016/j.jmapro.2021.06.070.

[48] Niu, S., Ma, Y., Lou, M., Zhang, C., & Li, Y. (2020). Joint formation mechanism and performance of resistance rivet welding (RRW) for aluminum alloy and press hardened steel. Journal of Materials Processing Technology, 286, 116830. doi:10.1016/j.jmatprotec.2020.116830.

[49] Rasmussen, K. J. R., Khezri, M., Schafer, B. W., & Zhang, H. (2020). The mechanics of built-up cold-formed steel members. Thin-Walled Structures, 154, 106756. doi:10.1016/j.tws.2020.106756.

[50] Steau, E., Mahendran, M., & Ariyanayagam, A. (2021). Sequentially coupled structural modelling of LSF floor-ceiling systems. Journal of Constructional Steel Research, 187, 106972. doi:10.1016/j.jcsr.2021.106972.

[51] Xue, J., Ma, S., Chen, X., Wu, Q., & Akbar, M. (2023). Finite element modeling of assembling rivet-fastened rectangular hollow flange beams in bending. Journal of Constructional Steel Research, 211. doi:10.1016/j.jcsr.2023.108177.

[52] Steau, E., Mahendran, M., & Keerthan, P. (2015). Web crippling tests of Rivet Fastened Rectangular Hollow Flange Channel Beams under Two Flange Load Cases. Thin-Walled Structures, 95, 262–275. doi:10.1016/j.tws.2015.06.008.

[53] Keerthan, P., & Mahendran, M. (2016). Experimental study on web crippling strength of hollow flange channels under end-one-flange and interior-one-flange load cases. Advances in Structural Engineering, 19(6), 966–981. doi:10.1177/1369433216630462.

[54] Wanniarachchi, K. S., & Mahendran, M. (2017). Experimental study of the section moment capacity of cold-formed and screw-fastened rectangular hollow flange beams. Thin-Walled Structures, 119, 499–509. doi:10.1016/j.tws.2017.05.033.

[55] Ishqy, M. F. M., Wanniarachchi, S., & Pologanathan, K. (2022). Shear behaviour of screw fastened rectangular hollow flange beams with web openings. Journal of Constructional Steel Research, 189, 107019. doi:10.1016/j.jcsr.2021.107019.

[56] Maali, M. S., Tavlaşoğlu, M. E., & Maali, M. (2025). Experimental study on the cold-formed steel beam-to-column screw connections for seismic application. Structures, 72, 108173. doi:10.1016/j.istruc.2024.108173.

[57] Li, H., Shi, Y., Xiang, Y., & Ran, X. (2025). Shear behavior of screw connections: Experiment, analysis, and application in CFS trusses. Structures, 73, 108405. doi:10.1016/j.istruc.2025.108405.

[58] Ho, H. C., Chung, K. F., Huang, M. X., Nethercot, D. A., Liu, X., Jin, H., Wang, G. D., & Tian, Z. H. (2020). Mechanical properties of high strength S690 steel welded sections through tensile tests on heat-treated coupons. Journal of Constructional Steel Research, 166, 105922. doi:10.1016/j.jcsr.2019.105922.

[59] Cooray, K. ., & Tharmarajah, G. (2023). Durability of Cold Formed Steel Structures used in residential and industrial construction. Proceedings of the SLIIT International Conference on Engineering and Technology, 245–255. doi:10.54389/rica2325.

[60] Ye, J., Quan, G., Yun, X., Guo, X., & Chen, J. (2022). An improved and robust finite element model for simulation of thin-walled steel bolted connections. Engineering Structures, 250, 113368. doi:10.1016/j.engstruct.2021.113368.

[61] Eid, N., & Joó, A. L. (2023). Simplified numerical model development for advanced design of lightweight-concrete encased cold-formed steel shear wall panels. SN Applied Sciences, 5(12), 366. doi:10.1007/s42452-023-05590-7.

[62] Dar, M. A., Subramanian, N., Anbarasu, M., Ghowsi, A. F., Arif, P. A., & Dar, A. R. (2021). Testing and FE simulation of lightweight CFS composite built-up columns: Axial strength and deformation behaviour. Thin-Walled Structures, 167, 108222. doi:10.1016/j.tws.2021.108222.

[63] Elyasi, N., Shahzamanian, M., Lin, M., Westover, L., Li, Y., Kainat, M., Yoosef-Ghodsi, N., & Adeeb, S. (2021). Prediction of Tensile Strain Capacity for X52 Steel Pipeline Materials Using the Extended Finite Element Method. Applied Mechanics, 2(2), 209–225. doi:10.3390/applmech2020013.

[64] Pavatharini, P. (2022). Experimental and Analytical Study of Built Up section of Cold Formed Steel (CFS) by Bolted Connection. International Research Journal of Innovations in Engineering and Technology, 6(4), 86–93. doi:10.47001/IRJIET/2022.604018.

[65] Xin, R., Le, V. T., & Goo, N. S. (2022). Buckling identification in composite cylindrical shells with measured imperfections using a Multi-DIC method and finite element analysis. Thin-Walled Structures, 177, 109436. doi:10.1016/j.tws.2022.109436.